

Nonlinear Conformal Transformation for In Situ IR-Visible Detection of Orbital Angular Momentum

Yuan Liu, Wei Chen,* Yang Ming, Wang Zhang, Jie Tang, Rui Yuan, Wei Hu, and Yan-Qing Lu*

Linear conformal transformation provides an effective way to detect orbital angular momentum (OAM) of photons, and particularly, their coherent superposition states that are significant for OAM-based technologies. However, these methods have limited applicability—they are applied to single or few separated wavelengths and cannot achieve nondestructive detection—although those features are attractive for practical applications. Here, the second-harmonic spiral transformation is theoretically described and experimentally demonstrated through IR-visible detection of OAM states from 900 to 1400 nm, with a low energy loss of $\approx 10^{-6}$. Remarkably, a record high optical finesse of ≈ 5.52 is predicted and observed, indicating that a nonlinear enhancement factor resulting from OAM conservation significantly improves separation efficiency. Additionally, this scheme allows flexibility to achieve lower energy losses or higher sensitivity by adjusting phase-matching conditions. These results can be applicable to classical and quantum areas and promote conformal transformation into nonlinear regions.

tweezers,^[2] telecommunication,^[3,4] super-resolution imaging,^[5] and quantum entanglement.^[6,7] Although it has been demonstrated that optical vortices can be generated by cylindrical lens pairs,^[1] spiral phase plates,^[8] computational holography,^[9] and *q*-plates,^[10] OAM detection is challenging because topological charges are veiled in their phases and cannot be directly distinguished.

The conventional OAM detection methods include interference and diffraction; the former distinguishes OAM modes with specific interference patterns of optical vortices carrying different OAM with reference beams^[9] (it can also be the vortex beam itself^[11]), and the latter uses various optical devices to convert the OAM beams into other modes to

identify their topological charges.^[12,13] Meanwhile, OAM modes also could be efficiently distinguished by their optical scattering processes with the sub-wavelength scatterers, such as the dielectric sphere,^[14] chiral structure,^[15] and single silver nanowire.^[16] Unfortunately, most of these schemes cannot identify coherently superimposed optical vortices because all OAM modes are measured in the same optical path, which results in considerable crosstalk. Although the measurement of superimposed states can be achieved based on fork or vortex gratings^[17,18] by converting different OAM modes into Gaussian-like modes at specific diffraction orders, the corresponding efficiency is limited to $1/N$, where N is the dimension of the underlying OAM state space.

Ray-optics conformal transformation^[19] makes the detection of superimposed OAM modes with high efficiency possible. The earliest proposed scheme is the log-polar transformation,^[20] where the spiral wavefront of the input vortex is mapped from concentric circles into parallel lines in Cartesian coordinates through an unwrapper and then collimated by a corrector. Thus, OAM modes with different topological charges are converted into plane waves with different tilted angles, which can be focused on distinct positions in the Fourier plane of a lens. Subsequently, spiral transformation was proposed by replacing the concentric circles with spiral lines, thereby significantly improving separation efficiency via sharper peaks of transformed beams.^[21] Recently, the simultaneous detection of spin and OAM via momentum transformation has been demonstrated, further decreasing the number of utilized optical elements while bringing more crosstalk.^[22]


1. Introduction

Nowadays, it is well known that an optical vortex with a helical wavefront possesses orbital angular momentum (OAM) with a value of $\ell\hbar$ per photon, where \hbar is the Dirac constant and ℓ is the topological charge corresponding to the phase winding factor.^[1] The inherent orthogonality and infinity of OAM provide a new degree of freedom to manipulate light waves, which has been extensively investigated in diverse fields, such as optical

Y. Liu, W. Chen, Y. Ming, W. Zhang, R. Yuan, W. Hu, Y.-Q. Lu
National Laboratory of Solid State Microstructures
Key Laboratory of Intelligent Optical Sensing and Manipulation
College of Engineering and Applied Sciences
and Collaborative Innovation Center of Advanced Microstructures
Nanjing University
Nanjing 210093, China
E-mail: wchen@nju.edu.cn; yqlu@nju.edu.cn

Y. Ming
Department of Electrical and Computer Engineering
National University of Singapore
Singapore 117583, Singapore

J. Tang
Department of Physics
Nantong University
Nantong 226019, China

 The ORCID identification number(s) for the author(s) of this article can be found under <https://doi.org/10.1002/lpor.202200656>

DOI: 10.1002/lpor.202200656

On the other hand, almost all of the above methods can be regarded as strong coupling detection, which means that the measurement will inevitably disturb the OAM state under detection. Although the schemes for OAM detection have been investigated since the proposal of the concept of optical OAM, it was not until 2016 that the weak measurement of OAM was proposed theoretically,^[23] and subsequently, demonstrated experimentally.^[24] The in situ probing of intense vortex pulses has been reported very recently, where the corresponding energy loss is as small as 10 per 10¹⁵ photons.^[25] However, this scheme requires a complex system to obtain strong-field photoionization, which essentially limits its practicality. Another recent work is based on the nonlinear Dammann vortex grating, which allows visible in situ detection of broadband near-infrared (NIR) vortices with a relatively low energy loss of $\approx 10^{-5}$, but suffers from an efficiency of $1/N$ owing to the vortex grating structure.^[26] To date, there is no in situ detection scheme that can satisfy both high efficiency and broad applicability.

Here, we introduce a second-harmonic (SH) spiral transformation as a novel approach to realizing in situ detection of OAM modes, which could be considered as an extension of spiral transformation to nonlinear optics. We show that this combination provides a nonlinear enhancement factor $\gamma = 2$ via the conservation of OAM in the nonlinear process, further improving separation efficiency. We also show the theoretical feasibility of switching between in situ and high sensitivity detection realized by regulating the phase-matching condition, which is fundamentally different from other in situ detection schemes. Since the detection is performed in the SH band and the three-wave coupling process is naturally wideband, this scheme allows visible detection of broadband NIR vortices. More specifically, by carving the holographic pattern of the SH spiral transformation in a nonlinear lithium niobate (LN) crystal, we experimentally demonstrate this method with in situ IR-visible detection of OAM modes from 900 to 1400 nm. The optical finesse that can characterize separation efficiency reaches a record high value of 5.52 in the experiment compared with its linear counterpart of 2.6, confirming the predicted enhancement factor. We also observed a relatively low energy loss of 10^{-6} under the situation of phase-mismatching.

2. Working Principle

To better understand the SH spiral transformation, we first re-examine the linear spiral transform. To perform the spiral transformation, one element (unwrapper) with a modulated phase $Q_\omega(x, y)$ converts the incident vortex with a helical phase $\exp(i\ell_\omega\theta)$ into a beam with a transverse phase gradient, where $Q_\omega(x, y)$ can be expressed as^[21]

$$Q_\omega(x, y) = \frac{k_\omega\beta}{d_\omega(a^2 + 1)} \left[(ax + y) \ln\left(\frac{r}{r_0}\right) + (x - ay)\varphi - (ax + y) \right] - \frac{k_\omega r^2}{2d_\omega} \quad (1)$$

where $r = \sqrt{x^2 + y^2}$ and $\varphi = \arctan(y/x) + 2n\pi$ are the polar coordinates (n is the spiral turns). r_0 , a , and β are the scaling parameters, ω is the angular frequency, $k_\omega = 2\pi/\lambda_\omega$ is the wave vector,

and d_ω is the propagation distance. The transformed beam has a tilted plane wave phase of $\exp(i\ell_\omega v/\beta)$ on the output plane (u, v) that satisfies^[21]

$$u(r, \varphi) = \frac{\beta}{1 + a^2} \left[a\varphi - \ln\left(\frac{r}{r_0}\right) \right] \quad (2)$$

$$v(r, \varphi) = \frac{\beta}{1 + a^2} \left[\varphi + a \ln\left(\frac{r}{r_0}\right) \right]$$

Another element (the corrector) with a modulation phase $P_\omega(u, v)$ on the plane (u, v) completes the transformation^[21]

$$P_\omega(u, v) = \frac{k_\omega r_0 \beta}{d_\omega(a^2 + 1)} e^{\frac{au + v}{\beta}} \times \left[\sin\left(\frac{u - av}{\beta}\right) + a \cos\left(\frac{u - av}{\beta}\right) \right] - \frac{k_\omega(u^2 + v^2)}{2d_\omega} \quad (3)$$

As shown in **Figure 1a,b**, such transformation maps a spiral $r = r_0 \cdot \exp(a\varphi)$ (along the incident vortex) to a straight line with phase $\exp(i\ell_\omega v/\beta)$, which means that vortices with different topological charges ℓ_ω are mapped to sinc functions with different shifts ℓ_ω/β in the Fourier space, but with the same width $2/(n\beta)$. By using a lens with focal length f , one can project the Fourier space in the real space, thereby separating the OAM modes in specific vertical positions $\lambda_\omega \ell_\omega f / 2\pi\beta$ with width $\lambda_\omega f / n\pi\beta$ (**Figure 1c**). The spiral transformation significantly improves separation efficiency and suppresses crosstalk owing to the factor n (typically, $n \approx 3$), compared to the log-polar transformation.^[20]

Next, we turn to the SH spiral transformation, starting with a pump and SH wave with arbitrary envelopes A_ω and $A_{2\omega}$; $E_\omega(\vec{r}, \varphi, z) = A_\omega e^{i\ell_\omega\varphi + ik_\omega z}$ and $E_{2\omega}(\vec{r}, \varphi, z) = A_{2\omega} e^{i\vec{k}_{2\omega_1} \cdot \vec{r} + ik_{2\omega_2} z}$, where $\vec{k}_{2\omega_1}$ and $k_{2\omega_2}$ are the transverse and longitudinal wave vectors of the SH wave, respectively. The SH wave propagates at arbitrary angles; therefore, its wave vector has longitudinal and transverse components, whereas the pump only has a longitudinal wave vector according to the vertical incidence condition. Assuming that the pump illuminates a quadratic material (the nonlinear unwrapper) with a modulated phase $Q_\omega(x, y)$, we can obtain the SH wave via small-signal approximation^[27] and slowly varying envelope approximation^[28]

$$\frac{dA_{2\omega}}{dz} = \kappa A_\omega^2 e^{i2\ell_\omega\varphi} e^{i(2k_\omega - k_{2\omega_2})z} e^{iQ_\omega(x, y) - i\vec{k}_{2\omega_1} \cdot \vec{r}} \quad (4)$$

where κ denotes the nonlinear coupling coefficient. Since the spiral transformation is based on ray optics, and we mainly focus on paraxial propagation wave components ($|\vec{k}_{2\omega_1}| \ll k_{2\omega_2}$),^[27] we ignore the transverse phase term $e^{-i\vec{k}_{2\omega_1} \cdot \vec{r}}$ according to the nonlinear Huygens principle.^[29] Therefore, Equation (4) can be expressed as

$$A_{2\omega} \approx \kappa \frac{A_\omega^2 e^{i(2k_\omega - k_{2\omega_2})L}}{i(2k_{2\omega} - k_{\omega_2})L} e^{i2\ell_\omega\varphi} e^{iQ_\omega(x, y)} = A^Z e^{i2\ell_\omega\varphi} e^{iQ_\omega(x, y)} \quad (5)$$

where L is the propagation distance. Equation (5) indicates that this process can be considered as a linear spiral transformation of an SH vortex with helical phase $\exp(i\ell_{2\omega}\theta)$, where $\ell_{2\omega} = 2\ell_\omega$

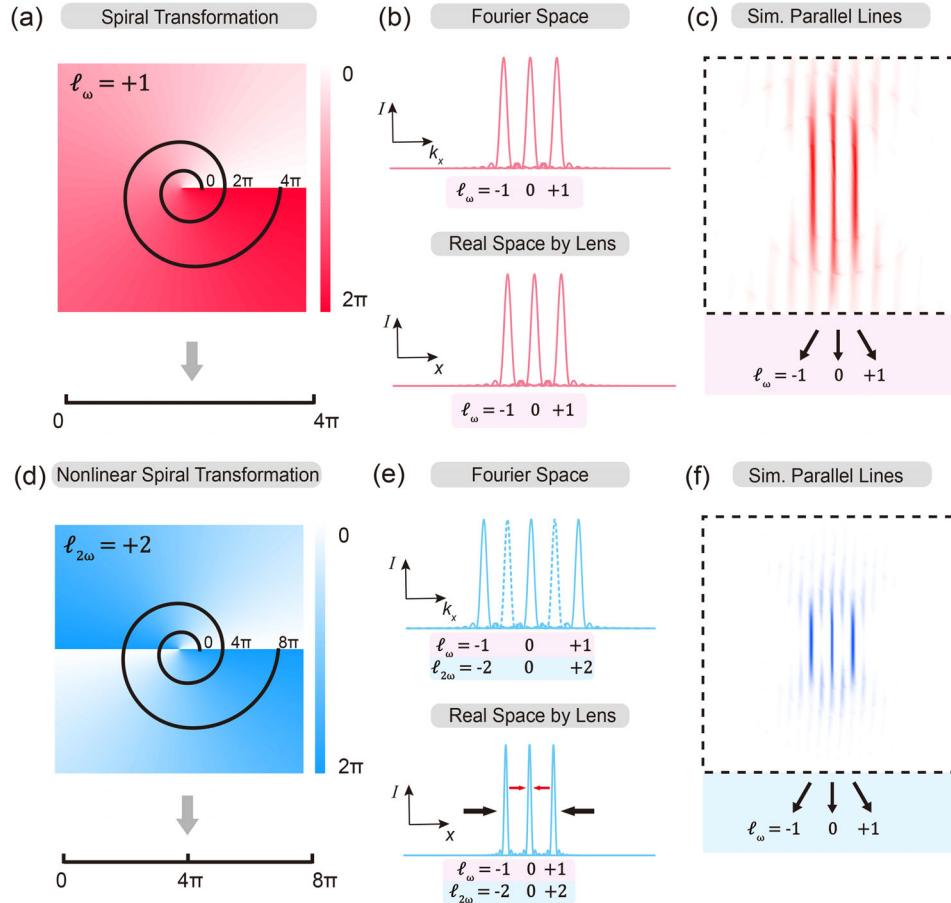


Figure 1. Comparison between linear and SH spiral transformations. a) Linear spiral transformation converts the incident vortex with a helical phase $\exp(i\ell_\omega\theta)$ into a beam with a transverse phase gradient $\exp(i\ell_\omega\nu/\beta)$. b) Fourier and real spaces projected by a lens. Note that “ I ” here indicates the intensity of the transformed beam and “ k_x ” refers to the spatial frequency corresponding to the x axis. c) Simulated results. d–f) Same as in (a–c) but for SH spiral transformation. Due to the enhancement factor γ , the SH spiral transformation greatly improves separation efficiency and further suppresses crosstalk.

(Figure 1d). Intuitively, this is the result of the OAM conservation in nonlinear interactions.^[28] It is worth mentioning that the phase-matching condition can be tailored by introducing a reciprocal vector in the z direction, thereby flexibly adjusting the intensity of the SH wave (shown in Figure S1, Supporting Information). Given that the transformation and correction phase patterns are unchanged for the SH vortex, we obtain

$$Q_{2\omega}(x, y) = \frac{k_{2\omega}\beta}{d_{2\omega}(a^2 + 1)} \left[(ax + y) \ln\left(\frac{r}{r_0}\right) + (x - ay)\theta - (ax + y) \right] - \frac{k_{2\omega}r^2}{2d_{2\omega}}$$

$$P_{2\omega}(u, v) = \frac{k_{2\omega}r_0\beta}{d_{2\omega}(a^2 + 1)} e^{\frac{au+v}{\beta}} \times \left[\sin\left(\frac{u-av}{\beta}\right) + a \cos\left(\frac{u-av}{\beta}\right) \right] - \frac{k_{2\omega}(u^2 + v^2)}{2d_{2\omega}} \quad (6)$$

where $d_{2\omega} = 2d_\omega$ to satisfy $Q_{2\omega}(x, y) = Q_\omega(x, y)$ and $P_{2\omega}(u, v) = P_\omega(u, v)$. One sees clearly that the SH vortex underwent a linear

spiral transformation with the same scaling parameters but double propagation distance $d_{2\omega}$. This means that in Fourier space, pump fundamental wave (FW) vortices with different topological charges ℓ_ω are mapped to sinc functions with shift $2\ell_\omega/\beta$ and width $2/(n\beta)$ (Figure 1e). In comparison with its linear counterpart, the SH spiral transformation further provides an enhancement factor of $\gamma = 2$ in mode shifts, which significantly improves separation efficiency (considering $n \approx 3$). Thus, one can separate the FW vortices (with the same lens) with different ℓ_ω in the same positions $\lambda_{2\omega}\ell_{2\omega}f/2\pi\beta = \lambda_\omega\ell_\omega f/2\pi\beta$, but with half-width, i.e., $\lambda_{2\omega}f/n\pi\beta = \lambda_\omega f/2n\pi\beta$ (the simulated results for comparing these two transformations are presented in Figure 1c,f). In addition to the enhancement factor γ , the SH spiral transformation has many other advantages, as demonstrated below.

3. Visible Detection of Infrared OAM With a Record High Separation Efficiency

For demonstration, we fabricated a nonlinear unwrapper from a 45 μm thick LN slice, whose nonlinear quadratic coefficient is modulated by $Q_{2\omega}(x, y)$, i.e., $\chi^{(2)}(x, y) = d_{ij}\text{sign}\{\cos[Q(x, y)]\}$, where $d_{ij} = d_{22}$ is an element of the second-order susceptibility

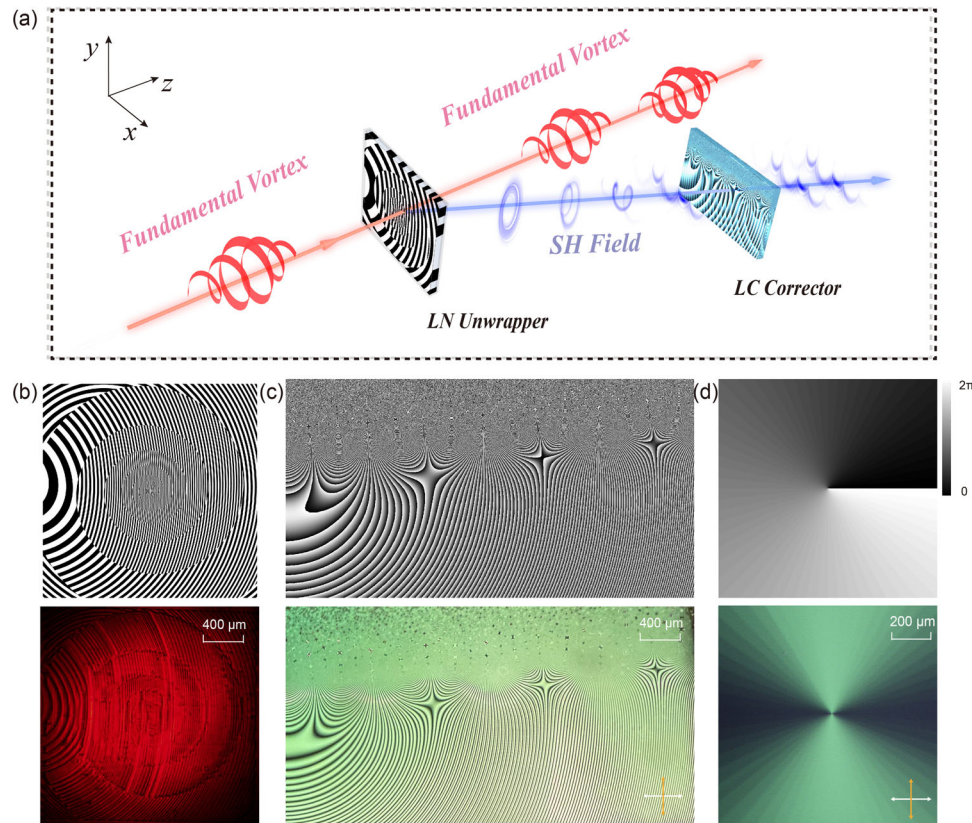


Figure 2. Schematic for SH spiral transformation process and samples used in the experiment. a) Process of NIR optical vortex detection through SH spiral transformation. b) Binary phase pattern of LN unwrapper (upper) and image of LN ferroelectric domain (lower). c) Accompanied LC corrector phase pattern (upper) and its image captured by polarized micrograph (lower). d) Phase pattern of LC q -plate (upper) and its image captured by polarized microscope (lower). The scale bars are given in (b–d). Double-ended arrows in (c) and (d) indicate the polarizer and analyzer, respectively.

$\chi^{(2)}$. This LN unwrapper is realized using the widely used electric field poling technique (Experimental Section),^[30] where the binary modulated $\chi^{(2)}$ can be expanded to a Fourier series, usually with a dominant term equal to $\exp(iQ_{2\omega})$.^[31] In addition, we fabricated a corrector from a nematic liquid crystal (LC) with its director profiles arranged by $P_{2\omega}(u, v)$ (Experimental Section),^[32] thereby contributing to the phase correction $\exp(iP_{2\omega})$. In our arrangement, the incident FW vortex propagates along the original path after interacting with the LN unwrapper while maintaining its mode, because the linear susceptibility of the LN unwrapper is not modulated (Figure 2a). Instead, the generated SH vortex undergoes a spiral transformation according to Equation (5) and is then modulated by the LC corrector. Notably, since one end of the converted straight line optical field is almost at the origin of the output plane (i.e., $u, v = 0$), the FW and SH waves naturally separate without the need for additional devices. The phase patterns for the LN unwrapper and LC corrector are shown in Figure 2b,c, respectively, in which the scaling parameters are $r_0 = 1.1$ mm, $2\pi a = \ln 1.6$, and $2\pi b = 1$ mm. The captured ferroelectric domain of the LN unwrapper (via SH imaging) and image of the LC corrector (via a polarized microscope) verified our design. Additionally, the FW vortices were generated by LC q -plates made in-house using the same technology as the LC corrector. The phase pattern and micrograph of a q -plate with $q = 0.5$ are shown in Figure 2d.

We note that the detection of OAM is performed in the SH wave band, which means that an NIR vortex can be converted into the visible band, and then, detected using a high-performance silicon-based charge coupled device (CCD) camera. In contrast, direct measurement based on the InGaAs detector suffers from some limitations, such as high readout noise, low speed response, and stringent cooling requirements.^[33] First, we chose $\lambda_\omega = 1400$ nm to verify this characteristic of SH spiral transformation. We carried out the experiment with a Ti:sapphire femtosecond laser (Revolution, Coherent, USA) pumped optical parametric amplifier (TOPAS-Prime, Light Conversion, Lithuania), which has a pulse duration of ≈ 50 fs and a repetition rate of 1 kHz. By alternating the right or left circular polarization states of the incident beam before the LC q -plates with $q = 0.5$ or 1, we obtain 1400 nm NIR optical vortices carrying opposite topological charges ($\ell_\omega = \pm 1$ and $\ell_\omega = \pm 2$) (Figure 3a). Figure 3d shows the simulated and experimental results after the incident optical vortices illuminated the LN unwrapper and then, propagated a distance of $2d_\omega \approx 90$ mm, where the NIR incident wavelength of $\lambda_\omega = 1400$ nm was converted to a visible wavelength of $\lambda_{2\omega} = 700$ nm through the SH generation process. The donut shapes of the optical vortices were transformed into long rectangular stripes with a length of ≈ 3.6 mm. These SH stripe-shaped fields were phase corrected to plane waves with a tilted phase by the LC corrector, and then a Fourier transform was applied

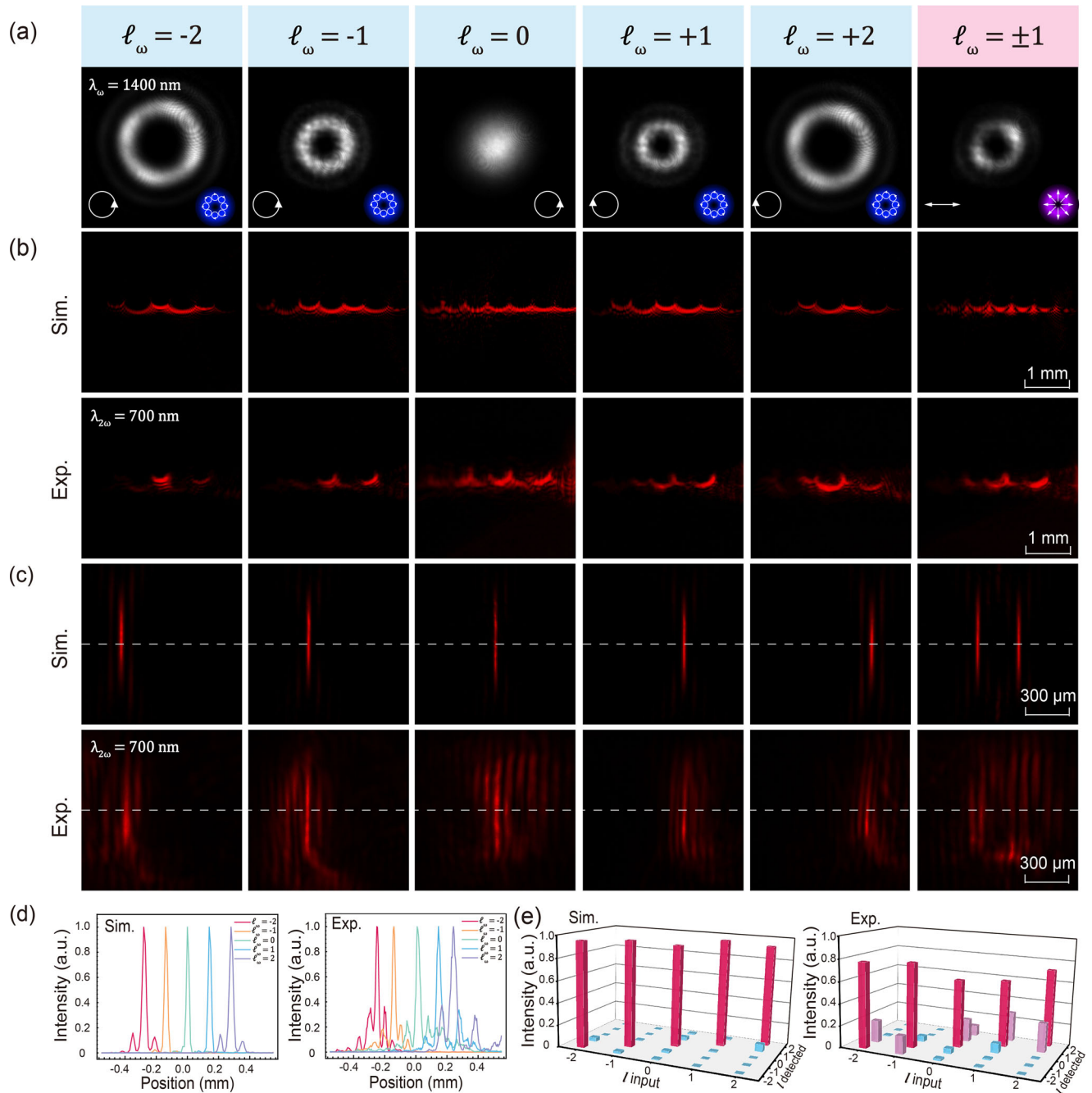


Figure 3. Simulated and experimental results of visible detection of IR OAM. a) Generated near-infrared (NIR) optical vortices carrying OAM of $\ell_\omega = -2$, $\ell_\omega = -1$, $\ell_\omega = 0$, $\ell_\omega = 1$, $\ell_\omega = 2$, and $\ell_\omega = \pm 1$ by LC q -plates. White arrows in the left corner indicate the polarization state of the incident Gaussian beam, and the right corner indicates the polarization distribution of generated optical vortices. b) Simulated and experimental SH unwrapped stripes of OAM beams passing through the LN unwrapper. c) Different OAM modes transformed to parallel lines at different vertical positions through the SH spiral transformation method. d) Intensity distribution along the dashed lines in (c). e) Crosstalk analysis of different sent and detected OAM modes calculated from (d).

by a spherical lens with $f = 100$ mm. Consequently, the adjacent NIR OAM modes were finally transformed into visible parallel lines with equal intervals determined by parameter β (Figure 3c). For the case of $\lambda_\omega = 1400$ nm, the separation interval was $S_{\ell_\omega+1} - S_{\ell_\omega} = \lambda_\omega f / 2\pi\beta \approx 140$ μm . Despite stray light, the experimental intensity profiles were consistent with the simulated re-

sults (Figure 3c). (The experimental detail especially the polarization configuration of the light can be found in Note S2, Supporting Information.) Furthermore, we generated a vector beam that simultaneously carried an OAM of $\ell_\omega = \pm 1$ by irradiating the LC q -plates with $q = 0.5$, with a linearly polarized incident beam. In this case, two vertical lines separated by ≈ 280 μm could

be distinguished, thus verifying the capability of detecting coherently superimposed OAM states via SH spiral transformation. Furthermore, no noticeable other nonlinear optical effects (such as the two-photon luminescence^[34]) are observed in the experiment, indicating that the SH generation dominates the whole nonlinear transformation process in the LN crystal.

Figure 3d shows the intensity profiles of these modes in the horizontal direction along the dashed middle lines, as shown in Figure 3c. Accordingly, we calculated the separation efficiency of SH spiral transformation, which can be quantified by the so-called optical finesse, defined as the ratio of the spacing between adjacent OAM states over their average full-width at half-maxima.^[35] As expected, this indicator reaches a record high value of 5.52 in experiment (6.30 for simulation) because of the nonlinear enhancement factor $\gamma = 2$ (shown in Figure S4, Supporting Information). This slight deviation between numerical and experimental values results from the practically transformed lines being slightly broader than the simulated ones owing to imperfect optical alignment. To analyze the crosstalk between different incident OAM modes varying from $\ell_\omega = -2$ to $\ell_\omega = 2$, we divided each OAM profile in Figure 3d into five equal parts and counted the intensity of each part, thereby determining the crosstalk from the power ratio of a specific OAM state.^[20,36] As shown in Figure 3e, the average power ratio of the detected OAM modes is $\approx 95.15\%$ in the simulation and 70.32% in the experiment. The difference between experimental results and simulation can be reduced by further adjusting the optical path so that the incident beams are strictly perpendicular to the LN unwrapper, and optimizing the binary strategy of $Q(x, y)$ to avoid the effect of stray light (shown in Figure S5, Supporting Information). Nevertheless, owing to the nonlinear enhancement factor, it is clearly available to determine the OAM state of NIR vortices from the sharp peak of the visible output line in the detector plane.

4. Broadband and Nondestructive Properties of SH Spiral Transformation

Further, we show the feasibility of wavelength demultiplexing of OAM modes owing to the broadband property of SH spiral transformation. Most of the reported conformal transformation schemes are limited to a single wavelength or several separated wavelengths because they are based on linear optical devices, such as spatial light modulator^[20,21] and metasurfaces.^[22,37] In contrast, the SH spiral transformation exhibits excellent wavelength compatibility owing to its nonlinear three-wave mixing process.^[27] Here, the detection of NIR optical vortices at wavelengths of $\lambda_\omega = 900$ nm and $\lambda_\omega = 1300$ nm was demonstrated. We only need to adjust the applied external electric field to LC devices for different wavelengths to satisfy the half-wave condition (Experimental Section) and change the distance between elements according to Equation (6). OAM modes with topological charges varying from -2 to $+2$ were transformed and captured, as shown in Figure 4a–c (shown in Figures S7 and S8, Supporting Information). Despite the optical vortices having the same topological charges, the position of transformed parallel lines varies with each other due to the difference between their wavelengths, i.e., $S_{\ell_\omega} = \lambda_\omega \ell_\omega f / 2\pi\beta$. Notably, the scales of the transformed lines decrease with the incident fundamental

wavelength owing to the same spherical lens ($f = 100$ mm) used to perform the spatial Fourier transform (more details are shown in Figure S6, Supporting Information). The intensity profiles along the dashed lines in both the simulation (Figure 4b) and experiment (Figure 4c) confirm that different OAM modes with separated wavelengths can be transformed to specific positions with a slight overlap, owing to the nonlinear enhancement factor. This means that demultiplexing of both the OAM and wavelength can be realized simultaneously by choosing suitable wavelength channels and scaling parameters of the SH spiral transformation. Although the demonstrated wavelength range of 500 nm is still much broader than previous results, the theoretical analysis clearly shows that a wider wavelength range is possible. In fact, despite the proposed nonlinear scheme has almost no wavelength limitation in theory, the bandwidth in practical application may be limited by other conditions, such as the transparency and working bandwidth of the LN and LC devices used in the experiment.

As mentioned previously, the LN unwrapper does not perturb the incident vortices owing to its modulation-free linear index. In addition, since the scheme unwraps the optical vortices from the center to the side and departs away from the original transmission direction (more strictly, just a tiny amount of overlap of FW and SH waves). Consequently, the generated SH stripes undergo phase correction and Fourier transform along a new path. The nondestructive property of SH spiral transformation is confirmed in Figure 4d, where the incident OAM mode ($\ell_\omega = -1$) is unchanged, as shown in the inserted captures measured before and after the LN unwrapper. As predicted by Equation (5), the corresponding converted SH OAM mode with doubled topological charge and half-wavelength was also captured on the surface of the LN unwrapper. We also quantified the energy loss of the input OAM modes, and the measured nonlinear conversion efficiencies are shown in Figure 4e,f. Since the intensity of the generated SH wave has a quadratic order dependence on the input beam intensity,^[27] the conversion efficiency has linear dependence on the incident power, with an order of magnitude of $\approx 10^{-6}$. Such low conversion efficiency results from the longitudinal wave vector mismatch, i.e., $\Delta k_z = k_\omega - k_{2\omega} \neq 0$ as described by Equation (5), indicating that this process can be regarded as in situ detection. Furthermore, the quasi-phase-matching mechanism can be introduced in the longitudinal direction via 3D domain engineering technology,^[38–40] thereby allowing us to make a trade-off between improving detection efficiency and reducing energy loss in practical applications.

5. Discussion and Conclusion

In this study, we have shown both theoretically and experimentally that in situ IR-visible detection of OAM modes can be achieved by SH spiral transformation. In comparison with previous optical transformation schemes, our proposed nonlinear strategy provides higher separation efficiency and better wavelength compatibility. Since the nonlinear enhancement factor ($\gamma = 2$) originates from the conservation of angular momentum in the nonlinear process, a similar mechanism can be used for higher separation efficiency by combining optical transformation with higher-order nonlinear effects, such as high-order harmonic

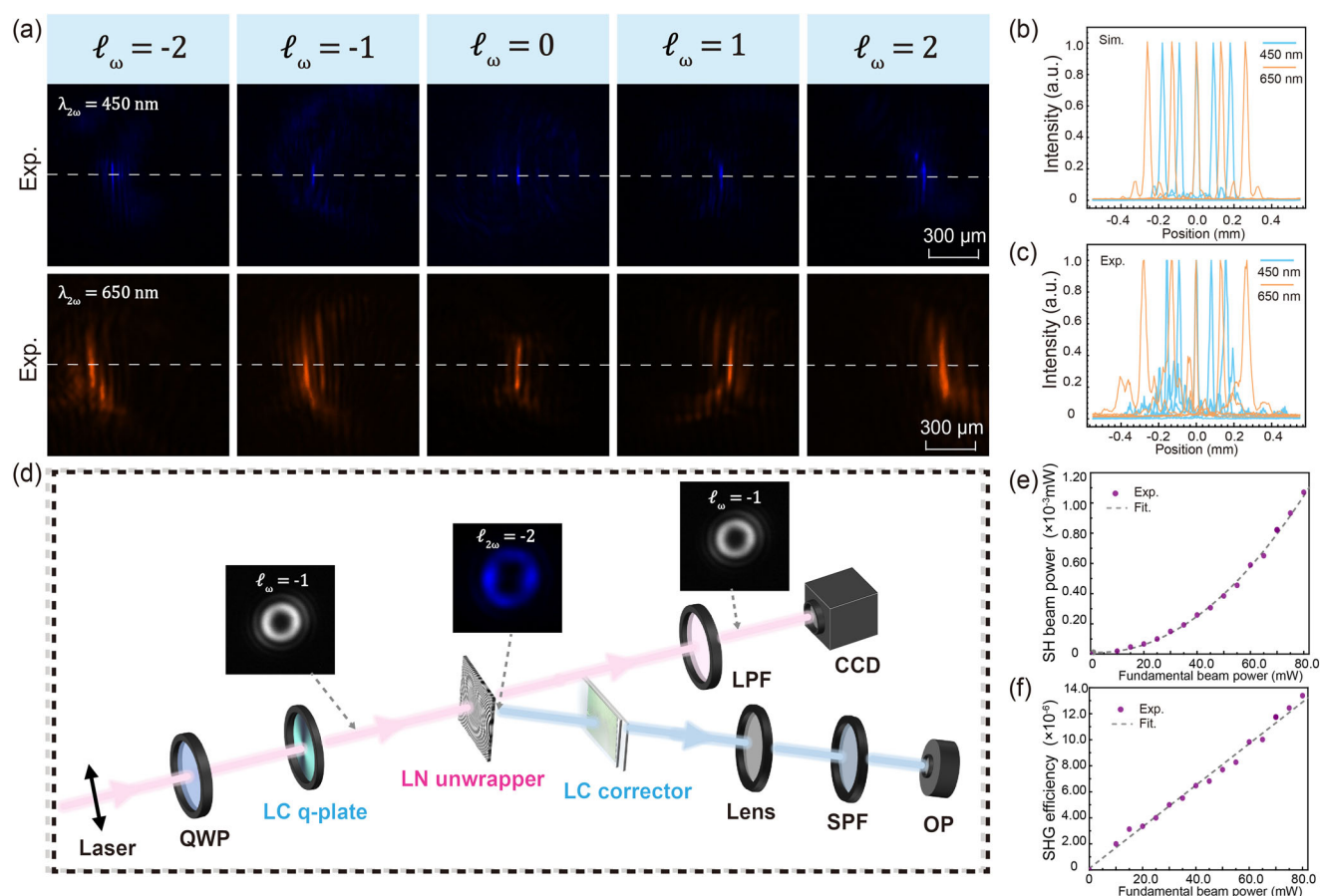


Figure 4. Broadband and nondestructive properties of SH spiral transformation. a) Experimental results for different incident wavelengths of $\lambda_{\omega} = 900$ nm and $\lambda_{2\omega} = 1300$ nm, and transformed parallel lines with SH wavelength of $\lambda_{2\omega} = 450$ nm and $\lambda_{2\omega} = 650$ nm. b, c) Simulated and experimental intensity profiles along the dashed lines in (a). d) Experimental setup to verify the nondestructive property of SH spiral transformation, where the input and output OAM modes are exhibited in the inserted captures. The red optical path marks the undisturbed FW vortices captured by a CCD camera. The blue optical path shows the transformed SH waves whose power is measured by an OP (QWP: quarter-wave plate, LPF: long pass filter, SPF: short pass filter, OP: optical powermeter). e, f) SH beam power and nonlinear conversion efficiency as a function of pump input beam power.

generation occurring in chirped nonlinear photonic crystals.^[41] By further introducing the sum frequency process,^[42] even visible detection of light at terahertz wavelength region can be expected. Both phase and amplitude information stored in terahertz photons is converted to the up-conversion photons through designed nonlinear conformal transformation process.^[43] Given that the nonlinear response is coherent and ultrafast in essence, this can allow spatial distinction of OAM modes loaded in different spectral components, which is attractive for optical communications. In addition, the limited sample processing accuracy (Figure 2b) may partly result in the observed crosstalk in the experiment, which can be reduced by the femtosecond laser processing technology with high precision.^[44] The crosstalk can also be suppressed by shifting the transformed SH wave to the first-order of the nonlinear Raman-Nath diffraction^[45] (shown in Figures S9, Supporting Information). Considering the previous effort for integrate d configuration based on linear spiral transformation,^[46] a similar compact scheme, such as the combination of the micro-structured LN slice and LC substrates, could be developed for detecting OAM modes through the proposed nonlinear conformal transformation.

We note that linear optical transformation based on geometric phase devices has enabled the simultaneous detection of both OAM and spin angular momentum (SAM).^[22] Similar detection is possible by performing SH spiral transformation through nonlinear metasurfaces owing to the nonlinear spin-orbit angular momentum interactions.^[47,48] Since the spin-determined geometric Berry phase is continuous, it can effectively suppress stray light in the current binary scheme. Given that such a nonlinear system maps different optical angular momentum to different spatial positions, the entanglement between optical path and total photon angular momentum can be generated through spontaneous parametric down-conversion,^[48,49] which can be used for high-dimensional quantum entanglement. Moreover, although research on linear conformal optics is growing rapidly,^[50–53] the investigation of nonlinear conformal transformation has lagged noticeably,^[54] particularly in the experimental aspect. Our results promote this research direction, and by further extending various conformal transformations to nonlinear optics, exotic phenomena and novel applications can be found in diverse fields, such as nonlinear beam shaping^[55] and invisible cloaks.^[56,57]

6. Experimental Section

Electrically Poling Fabrication and Observation of LN Unwrapper: Electrically poling process for the fabrication of LN unwrapper. An LN wafer with a 45 μm thickness was adopted. The wafer surface was first processed through plasma and ultrasonic cleaning. Then, the maskless photolithography, vacuum deposition, and photoresist removal procedures transformed the phase mask of the binary unwrapper to a +z surface with a 120 nm Cr electrode. Finally, a high voltage of 1160 V was applied to the Cr electrode, resulting in the reversed LN domain with opposite spontaneous polarization directions. The LN unwrapper was accomplished by removing the Cr electrode. The fabricated LN unwrapper domain was observed in the experimental setup through the SH generation process with the help of a 4f system, as shown in Figure 2b.

Photoalignment Technology for the Fabrication of LC Corrector: Indium-tin-oxide glass substrates ($1.5 \times 2 \text{ cm}^2$) were ultrasonically and UV-Ozone cleaned and then spin-coated with the polarization-sensitive photoalignment agent SD1 (Dai-Nippon Ink and Chemicals, Japan), which was dissolved in dimethylformamide (DMF) at a concentration of 0.3 wt%. After curing at 100 $^\circ\text{C}$ for 10 min, two pieces of glass substrates were assembled into a cell using UV curing adhesive with 6 μm spacers mixed. A multistep partly overlapping exposure process was performed to carry out space-variant orientations of SD1 matching with the designed corrector's phase through a digital micromirror device-based dynamic microlithography system. After yelling the photoaligned cell with nematic LC E7 (HCCH, China), LC molecules followed the direction of SD1 orientations, and the LC corrector was thereby accomplished. The fabricated LC corrector was observed by polarized microscope, as shown in Figure 2c. The phase retardation of the LC corrector could be expressed as $\Gamma = 2\pi(n_{\text{eff}} - n_o)d_{\text{LC}}/\lambda$, where n_{eff} changed from n_e to n_o with the applied electric field due to LC molecule tilting. For different wavelength in the experiment, corresponding external voltage of 1 kHz square wave with different voltage $V = 2.3 \text{ V}$ for $\lambda_{2\omega} = 700$ and 650 nm, $V = 2.8 \text{ V}$ for $\lambda_{2\omega} = 450 \text{ nm}$ was adopted.

Simulation for Linear Propagation of Beams: After the LN unwrapper, the following propagation of the SH wave was the linear process, which could be calculated with the discrete angular spectrum method.^[58] $A_{2\omega}(k_x, k_y, 0)$ was defined as the Fourier transformation of the SH wave $A_{2\omega}(x, y, 0)$, and the SH wave after propagation with a distance of d could be calculated by

$$A_{2\omega}(k_x, k_y, 0) = \iint A_{2\omega}(x, y, 0) \cdot e^{-i2\pi(xk_x + yk_y)} dx dy$$

$$A_{2\omega}(x, y, d) = \iint A_{2\omega}(k_x, k_y, 0) \cdot e^{id\sqrt{k^2 - 4\pi^2(k_x^2 + k_y^2)}} \cdot e^{i2\pi(xk_x + yk_y)} dk_x dk_y$$
(7)

where k_x and k_y are the transverse wavevectors of the SH wave.

Supporting Information

Supporting Information is available from the Wiley Online Library or from the author.

Acknowledgements

Y.L. and W.C. contributed equally to this work. The work was supported by the Natural Science Foundation of Jiangsu Province, Major Project (BK20212004); Innovation Program for Quantum Science and Technology (2021ZD0301500); and the National Natural Science Foundation of China (NSFC) (62035008, 12004200).

Conflict of Interest

The authors declare no conflict of interest.

Data Availability Statement

The data that support the findings of this study are available from the corresponding author upon reasonable request.

Keywords

conformal transformation, IR-visible detection, nonlinear photonic crystals, orbital angular momentum

Received: August 29, 2022
Revised: November 9, 2022
Published online: January 29, 2023

- [1] L. Allen, M. W. Beijersbergen, R. J. C. Spreeuw, J. P. Woerdman, *Phys. Rev. A* **1992**, *45*, 8185.
- [2] M. Padgett, R. Bowman, *Nat. Photonics* **2011**, *5*, 343.
- [3] J. Wang, J. Y. Yang, I. M. Fazal, N. Ahmed, Y. Yan, H. Huang, Y. Ren, Y. Yue, S. Dolinar, M. Tur, A. E. Willner, *Nat. Photonics* **2012**, *6*, 488.
- [4] N. Bozinovic, Y. Yue, Y. Ren, M. Tur, P. Kristensen, H. Huang, A. E. Willner, S. Ramachandran, *Science* **2013**, *340*, 1545.
- [5] L. Yan, P. Gregg, E. Karimi, A. Rubano, L. Marrucci, R. Boyd, S. Ramachandran, *Optica* **2015**, *2*, 900.
- [6] A. Mair, A. Vaziri, G. Weihs, A. Zeilinger, *Nature* **2001**, *412*, 313.
- [7] M. Erhard, M. Krenn, A. Zeilinger, *Nat. Rev. Phys.* **2020**, *2*, 365.
- [8] S. S. R. Oemrawsingh, J. A. W. van Houwelingen, E. R. Eliel, J. P. Woerdman, E. J. K. Versteegen, J. G. Kloosterboer, G. W. 't Hooft, *Appl. Opt.* **2004**, *43*, 688.
- [9] N. R. Heckenberg, R. McDuff, C. P. Smith, A. G. White, *Opt. Lett.* **1992**, *17*, 221.
- [10] L. Marrucci, C. Manzo, D. Paparo, *Phys. Rev. Lett.* **2006**, *96*, 163905.
- [11] J. Leach, M. J. Padgett, S. M. Barnett, S. Franke-Arnold, J. Courtial, *Phys. Rev. Lett.* **2002**, *88*, 257901.
- [12] G. C. G. Berkhout, M. W. Beijersbergen, *Phys. Rev. Lett.* **2008**, *101*, 100801.
- [13] J. M. Hickmann, E. J. S. Fonseca, W. C. Soares, S. Chávez-Cerda, *Phys. Rev. Lett.* **2010**, *105*, 053904.
- [14] V. Garbin, G. Volpe, E. Ferrari, M. Versluis, D. Cojoc, D. Petrov, *New J. Phys.* **2009**, *11*, 013046.
- [15] T. Lei, M. Zhang, Y. Li, P. Jia, G. N. Liu, X. Xu, Z. Li, C. Min, J. Lin, C. Yu, H. Niu, X. Yuan, *Light: Sci. Appl.* **2015**, *4*, e257.
- [16] D. Paul, D. K. Sharma, G. V. P. Kumar, *Laser Photonics Rev.* **2022**, *16*, 2200049.
- [17] N. Zhang, X. C. Yuan, R. E. Burge, *Opt. Lett.* **2010**, *35*, 3495.
- [18] P. Woźniak, I. De Leon, K. Höflich, G. Leuchs, P. Banzer, *Optica* **2019**, *6*, 961.
- [19] W. J. Hossack, A. M. Darling, A. Dahdouh, *J. Mod. Opt.* **1987**, *34*, 1235.
- [20] G. C. G. Berkhout, M. P. J. Lavery, J. Courtial, M. W. Beijersbergen, M. J. Padgett, *Phys. Rev. Lett.* **2010**, *105*, 153601.
- [21] Y. Wen, I. Chremmos, Y. Chen, J. Zhu, Y. Zhang, S. Yu, *Phys. Rev. Lett.* **2018**, *120*, 193904.
- [22] Y. Guo, S. Zhang, M. Pu, Q. He, J. Jin, M. Xu, Y. Zhang, P. Gao, X. Luo, *Light: Sci. Appl.* **2021**, *10*, 63.
- [23] J. Qiu, C. Ren, Z. Zhang, *Phys. Rev. A* **2016**, *93*, 063841.
- [24] J. Zhu, P. Zhang, Q. Li, F. Wang, C. Wang, Y. Zhou, J. Wang, H. Gao, L. C. Kwek, F. Li, *Sci. Rep.* **2019**, *9*, 7993.
- [25] Y. Fang, Z. Guo, P. Ge, Y. Dou, Y. Deng, Q. Gong, Y. Liu, *Light: Sci. Appl.* **2022**, *11*, 34.
- [26] Y. Liu, W. Chen, W. Zhang, C.-Q. Ma, H.-X. Chen, Y.-F. Xiong, R. Yuan, J. Tang, P. Chen, W. Hu, F. Xu, Y. Q. Lu, *Adv. Opt. Mater.* **2022**, *10*, 2101098.

- [27] R. W. Boyd, *Nonlinear Optics*, Academic Press, San Diego, CA **2019**.
- [28] N. V. Bloch, K. Shemer, A. Shapira, R. Shiloh, I. Juwiler, A. Arie, *Phys. Rev. Lett.* **2012**, *108*, 233902.
- [29] Y. Q. Qin, C. Zhang, Y. Y. Zhu, X. P. Hu, G. Zhao, *Phys. Rev. Lett.* **2008**, *100*, 063902.
- [30] Y. Liu, W. Chen, J. Tang, X. Xu, P. Chen, C.-Q. Ma, W. Zhang, B.-Y. Wei, Y. Ming, G. X. Cui, Y. Zhang, W. Hu, Y. Q. Lu, *Adv. Opt. Mater.* **2021**, *9*, 2001776.
- [31] T. Ellenbogen, N. Voloch-Bloch, A. Ganany-Padowicz, A. Arie, *Nat. Photonics* **2009**, *3*, 395.
- [32] Z. X. Li, Y. P. Ruan, P. Chen, J. Tang, W. Hu, K. Y. Xia, Y. Q. Lu, *Chin. Opt. Lett.* **2021**, *19*, 112601.
- [33] A. Rogalski, *Infrared Phys. Technol.* **2002**, *43*, 187.
- [34] F. Auzel, *Chem. Rev.* **2004**, *104*, 139.
- [35] C. Wan, J. Chen, Q. Zhan, *APL Photonics* **2017**, *2*, 031302.
- [36] M. Mirhosseini, M. Malik, Z. Shi, R. W. Boyd, *Nat. Commun.* **2013**, *4*, 2781.
- [37] B. Wang, Y. Wen, J. Zhu, Y. Chen, S. Yu, *Opt. Express* **2020**, *28*, 16342.
- [38] D. Wei, C. Wang, H. Wang, X. Hu, D. Wei, X. Fang, Y. Zhang, D. Wu, Y. Hue, J. Lie, S. Zhu, M. Xiao, *Nat. Photonics* **2018**, *12*, 596.
- [39] T. Xu, K. Switkowski, X. Chen, S. Liu, K. Koynov, H. Yu, H. Zhang, J. Wang, Y. Sheng, W. Krolikowski, *Nat. Photonics* **2018**, *12*, 591.
- [40] D. Wei, C. Wang, X. Xu, H. Wang, Y. Hu, P. Chen, J. Li, Y. Zhu, C. Xin, X. Hu, Y. Zhang, D. Wu, J. Chu, S. Zhu, M. Xiao, *Nat. Commun.* **2019**, *10*, 4193.
- [41] B.-Q. Chen, C. Zhang, C.-Y. Hu, R.-J. Liu, Z.-Y. Li, *Phys. Rev. Lett.* **2015**, *115*, 083902.
- [42] K. Nawata, T. Notake, H. Ishizuki, Y. Takida, Y. Tokizane, S. Hayashi, Z. Han, T. Taira, H. Minamide, in *2015 40th Int. Conf. Infrared, Millimeter, and Terahertz Waves (IRMMW-THz)*, Hong Kong, China, **2015**, pp. 1–2.
- [43] D. Nicoletti, A. Cavalleri, *Adv. Opt. Photonics* **2016**, *8*, 401.
- [44] B. Zhu, X. Liu, H. Liu, Y. A. Liu, X. Yan, Y. Chen, X. Chen, *Phys. Status Solidi RRL* **2020**, *14*, 2000213.
- [45] S. M. Saltiel, D. N. Neshev, W. Krolikowski, A. Arie, O. Bang, Y. S. Kivshar, *Opt. Lett.* **2009**, *34*, 848.
- [46] Y. Wen, I. Chremmos, Y. Chen, G. Zhu, J. Zhang, J. Zhu, Y. Zhang, J. Liu, S. Yu, *Optica* **2020**, *7*, 254.
- [47] J. C. Howell, R. S. Bennink, S. J. Bentley, R. W. Boyd, *Phys. Rev. Lett.* **2004**, *92*, 210403.
- [48] Y. Ming, W. Zhang, J. Tang, Y. Liu, Z. Xia, Y. Liu, Y. Q. Lu, *Laser Photonics Rev.* **2020**, *14*, 1900146.
- [49] T. J. Herzog, P. G. Kwiat, H. Weinfurter, A. Zeilinger, *Phys. Rev. Lett.* **1995**, *75*, 3034.
- [50] H. Chen, C. T. Chan, P. Sheng, *Nat. Mater.* **2010**, *9*, 387.
- [51] J. B. Pendry, A. Aubry, D. R. Smith, S. A. Maier, *Science* **2012**, *337*, 549.
- [52] L. Xu, H. Chen, *Nat. Photonics* **2015**, *9*, 15.
- [53] J. Zhang, J. Pendry, Y. Luo, *Adv. Photonics* **2019**, *1*, 014001.
- [54] O. Paul, M. Rahm, *Opt. Express* **2012**, *20*, 8982.
- [55] X. Hu, Y. Zhang, S. Zhu, *Adv. Mater.* **2020**, *32*, 1903775.
- [56] U. Leonhardt, *Science* **2006**, *312*, 1777.
- [57] J. B. Pendry, D. Schurig, D. R. Smith, *Science* **2006**, *312*, 1780.
- [58] J. W. Goodman, *Introduction to Fourier Optics*, 3rd ed., Academic Press, San Diego, CA **2005**.